Delayed feedback control of stochastic spatiotemporal dynamics in a resonant tunneling diode

G. Stegemann,* A. G. Balanov,† and E. Schöll‡
Institut für Theoretische Physik, Technische Universität Berlin, D-10623 Berlin, Germany
(Received 21 July 2005; published 5 January 2006)

The influence of time-delayed feedback upon the spatiotemporal current density patterns is investigated in a model of a semiconductor nanostructure, namely a double-barrier resonant tunneling diode. The parameters are chosen below the Hopf bifurcation, where the only stable state of the system is a spatially inhomogeneous "filamentary" steady state. The addition of weak Gaussian white noise to the system gives rise to spatially inhomogeneous self-sustained temporal oscillations that can be quite coherent. We show that applying a time-delayed feedback can either increase or decrease the regularity of the noise-induced dynamics in this spatially extended system. Using linear stability analysis, we can explain these effects, depending on the length of the delay interval. Furthermore, we study the influence of this additional control term upon the deterministic behavior of the system, which can change significantly depending on the choice of parameters.

DOI: 10.1103/PhysRevE.73.016203 PACS number(s): 05.45.−a, 05.40.−a, 72.20.Ht, 72.70.+m

I. INTRODUCTION

The double-barrier resonant tunneling diode (DBRT) is a semiconductor device, whose nonlinear conduction properties are based upon quantum-mechanical phenomena [1]. Usually it consists of an undoped double-barrier heterostructure sandwiched between two doped contact areas that serve as emitter and collector, respectively. Quantum confinement in the quantum well between the two barriers leads to discrete energy levels for the electrons. Applying a voltage to the device gives rise to a current between the emitter and collector, and if the energy of the incoming electrons coincides with the energy levels in the well, resonant tunneling occurs [2]. These resonances can lead to negative differential conductivity [3]. The properties of charge accumulation in the quantum well can result in a Z-shaped current-voltage characteristic where in a range of voltages three steady states exist [4,5]. Since resonant tunneling is a very fast process, the DBRT turns out to be promising for high-speed electronics, e.g., as a picosecond switch [6] or as a very high-frequency microwave generator with a potential operating range up to several THz [7].

It was shown that the lateral redistribution of charge carriers in the quantum well of the DBRT can lead to a variety of self-organized spatiotemporal patterns of the current density [5,8–13], including quite irregular breathing and spiking patterns [14].

The presence of random fluctuations can seriously affect charge transport in semiconductors [15], which usually leads to deterioration of their performance. However, recently the constructive role of noise in semiconductor devices has been recognized. In particular, noise in semiconductor lasers was shown to induce coherent radiation [16–18], whereas in resonant tunneling diodes it can generate quite regular charge transport dynamics, and even lead to spatial homogenization of current density patterns [19].

Generally, noise-induced dynamics depends on the statistics of random fluctuations and their intensity, which are not easily accessible in real practical situation. In [20,21], a method for manipulation of essential features of noise-induced oscillations was proposed using a delayed feedback scheme that was originally used to control chaos in purely deterministic systems [22]. This technique was demonstrated to be effective for control of noise-induced oscillations in simple systems close to either local or global instabilities. In the present work, we study the effect of delayed feedback on the stochastic spatiotemporal pattern formation in the DBRT model for parameter values close to, but below, a Hopf bifurcation. We show that using this method, one can control both the time scales and the coherence of noise-induced current density patterns in semiconductor devices. Moreover, if the feedback strength is large, it might induce a Hopf bifurcation, which leads to the emergence of periodic patterns, whose spatial properties depend on the feedback strength and the noise intensity.

The paper is organized as follows. In Sec. II, the DRBT model is described, and noise-induced patterns that appear below the Hopf bifurcation are discussed. Section III is devoted to effects of delayed feedback upon noise-induced dynamics in the DBRT. In Sec. IV, we draw conclusions.

II. NOISE-INDUCED PATTERN FORMATION

In our study, we use a deterministic model for the DBRT suggested in [14] with two sources of random fluctuations added as proposed in [19], [1]

$$\frac{\partial a(x,t)}{\partial t} = f(a,u) + \frac{\partial}{\partial x}\left(D(a)\frac{\partial a}{\partial x}\right) + D_a\xi(x,t),$$

$$\frac{\partial u(t)}{\partial t} = \frac{1}{\varepsilon}(U_0 - u - rJ) + D_u\eta(t), \qquad (1)$$

where all quantities are dimensionless. From the viewpoint of nonlinear dynamics, this is a reaction-diffusion model of

*Electronic address: stegemann@physik.tu-berlin.de
†Electronic address: balanov@physik.tu-berlin.de
‡Electronic address: schoell@physik.tu-berlin.de

[1] Herewith a misprint in Eq. (1) of [19], which gives an erroneous scaling factor ε in the D_u term, is corrected.

activator-inhibitor type, where a is the activator and u is the inhibitor. The dynamical variable $a(x,t)$ depends on time and space and describes the charge-carrier density inside the quantum well in typical units of $10^{10}/\mathrm{cm}^2$, whereas the second variable $u(t)$ depends only on time and is the voltage drop across the device in typical units of 0.35 mV. The net tunneling rate of the electrons through the two energy barriers into and out of the quantum well is modeled by the nonlinear function $f(a,u)$. $D(a)$ is an effective diffusion coefficient and describes the diffusion of the electrons within the quantum well perpendicular to the current flow (along the x direction). $J=(1/L)\int_0^L j dx$ gives the total current through the device in typical units of $500\ \mathrm{A/cm}^2$, where $j(a,u)=\frac{1}{2}[f(a,u)+2a]$ is the local current density within the well. The system's width is fixed at a value of $L=30$ and homogeneous Neumann boundary conditions are used. The first Eq. (1) is the local balance equation of the charge in the quantum well, and the second equation represents Kirchhoff's law of the circuit in which the device is operated. The control parameters are the external bias voltage U_0, the dimensionless load resistance r, and ε. The latter, describing the time-scale ratio of the dynamics of u and a, plays the role of a bifurcation parameter which determines the stability of the fixed points in the system [23]. Physically, $\varepsilon=RC/\tau_a$ is related to the load resistance R and the parallel capacitance C of the attached circuit, normalized by the tunneling time τ_a. The explicit form of the functions $f(a,u)$ and $D(a)$ is given in the Appendix and a discussion of the various deterministic bifurcation scenarios can be found in [14,23]. In Eq. (1), we use uncorrelated Gaussian white noise sources ξ and η with noise intensities D_a and D_u in the respective variables,

$$\langle \xi(x,t)\rangle = \langle \eta(t)\rangle = 0 \quad (x \in [0,L]),$$

$$\langle \xi(x,t)\xi(x',t')\rangle = \delta(x-x')\delta(t-t'),$$

$$\langle \eta(t)\eta(t')\rangle = \delta(t-t'). \tag{2}$$

In the noise-free case, $D_u=D_a=0$, one can calculate the null isoclines of the system. These are plotted in Fig. 1 using the current-voltage projection of the originally infinite-dimensional phase space. There are three curves, namely the null isocline $\dot{u}=0$ (i.e., the *load line*) and two null isoclines $\dot{a}=0$, one for a reduced system, including only spatially homogeneous states, and one for the full system. We call the system *spatially homogeneous* if the space dependent variable $a(x,t)$ is uniformly distributed over the whole width of the device, i.e., $a(x,t)=a(t)$ for all $x \in [0,L]$, otherwise it is called *spatially inhomogeneous*.

In Fig. 1, one can see the Z-shaped current-voltage characteristic of the DBRT (solid curve), and the inset represents our special region of interest for the following investigations. We fix $\varepsilon=6.2$ slightly below the Hopf bifurcation, which occurs at $\varepsilon_{\mathrm{Hopf}} \approx 6.469$. In this regime we have a stable, spatially inhomogeneous fixed point marked "*I*" in Fig. 1, which is determined by the intersection of the load line (null isocline $\dot{u}=0$) with the nullcline $\dot{a}=0$ for inhomogeneous $a(x,t)$. The neighboring intersection of the load line with the homogeneous nullcline (marked "*H*") defines another, spatially homogeneous fixed point which is a saddle. It is stable with respect to completely homogeneous perturbations but generally unstable against spatially inhomogeneous fluctuations.

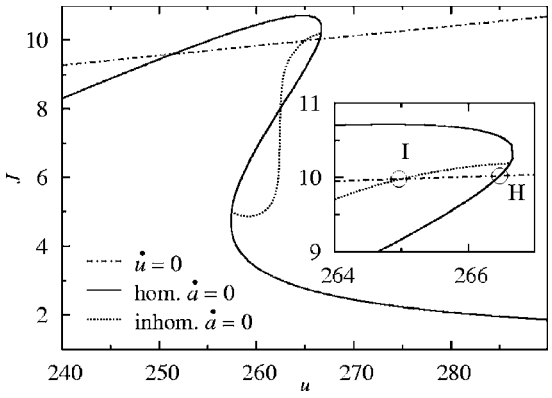

FIG. 1. Current-voltage characteristic of the DBRT model. The null isoclines for the dynamical variables u (which is denoted by the load line, dash-dotted) and a in the case of a homogeneous $a(x)$ (solid) and in the case of inhomogeneous $a(x)$ (dotted) are shown. The inset shows an enlargement, where I and H mark the inhomogeneous and the homogeneous fixed points of the system, respectively. $U_0=-84.2895$, $r=-35$. Other parameters as in [19,23]. This gives typical units of $500\ \mathrm{A/cm}^2$ for the current density and 0.35 mV for the voltage.

We have previously shown that the addition of noise can induce various spatiotemporal patterns in the system [19]. If we fix the spatially inhomogeneous random perturbations of the variable a at a small noise intensity of $D_a=10^{-4}$ and investigate the behavior of the system under variation of the noise intensity D_u, we can observe the different spatiotemporal scenarios shown in Fig. 2. Note that this noise term does not have any space-dependent influence upon a. Never-

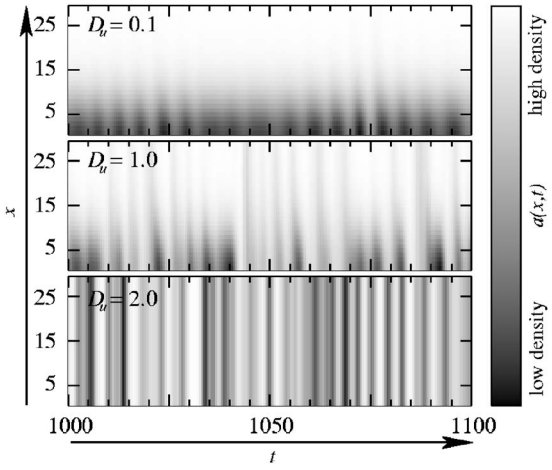

FIG. 2. Spatiotemporal patterns $a(x,t)$ induced by different noise intensities $D_u=0.1, 1.0, 2.0$. At $t=0$, the system is prepared in the spatially inhomogeneous steady state "*I*" and with the parameters of Fig. 1. The system is then simulated with $D_a=10^{-4}$ and D_u as indicated. $U_0=-84.2895$, $r=-35$, $\varepsilon=6.2$. Time t and space x are measured in units of the tunneling time τ_a and the diffusion length l_a, respectively. Typical values at 4 K are $\tau_a=3.3$ ps and $l_a=100$ nm [23].

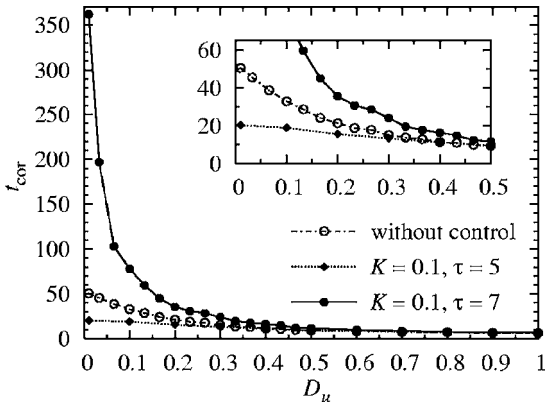

FIG. 3. Correlation time vs noise intensity D_u without control ($K=0$) and with control and two different values of τ as indicated. Averages from 100 time series of length $T=10\,000$, parameters as in Fig. 2. The inset shows an enlargement.

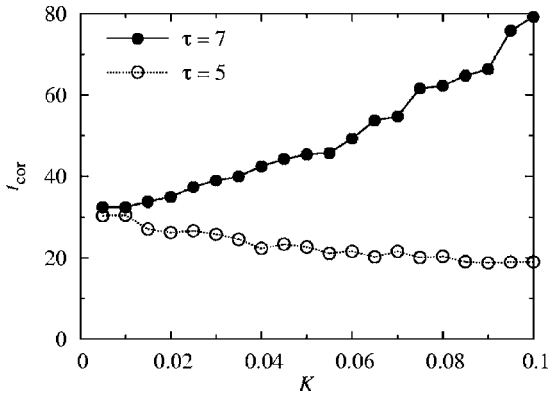

FIG. 4. Correlation time vs feedback strength K for $\tau=5$ and $\tau=7$. $D_u=0.1$, $D_a=10^{-4}$. Calculated as in Fig. 3.

theless the noise-induced spatiotemporal dynamics changes with increasing D_u from quite regular spatially inhomogeneous breathing oscillations around the inhomogeneous fixed point ($D_u=0.1$, upper panel in Fig. 2) into a *mixed mode* of alternating homogeneous and inhomogeneous states ($D_u=1$, middle panel) and finally turns into a completely homogeneous behavior ($D_u=2$, lower panel).

Physically, D_u can be realized by an external tunable noise voltage source in parallel with the supply bias, as used experimentally, e.g., in [17]. In typical dimensional units of $\varepsilon k_B T/e$ [14], $D_u=1$ corresponds to a parallel noise voltage of 2 mV at $T=4$ K. D_a describes internal fluctuations of the local current density which could be caused, e.g., by shot noise [15]. The small value of $D_a=10^{-4}$ used in our simulation gives a noise current density of the order of 50 mA/cm^2, which is within the range of Poissonian shot noise currents $\sqrt{2e\langle I\rangle/\tau_a}$, where $\langle I\rangle$ ist the global mean current.

To measure the temporal ordering of the system, we use the correlation time [24] calculated from the voltage signal u,

$$t_{\mathrm{cor}} \equiv \frac{1}{\sigma^2}\int_0^\infty |\Psi(s)|ds, \tag{3}$$

where $\Psi(s)\equiv\langle[u(t)-\langle u\rangle][u(t+s)-\langle u\rangle]\rangle_t$ is the autocorrelation function of the variable $u(t)$ and $\sigma^2=\Psi(0)$ is its variance.

This correlation time is plotted in Fig. 3. Here (referring to the graph "without control") one can see, as expected, that the temporal coherence of the oscillations decreases rapidly with increasing noise intensity D_u.

In summary, noise induces oscillations in the system, which would otherwise rest in its inhomogeneous fixed point. With growing noise intensity, the dynamics changes from small inhomogeneous oscillations that are quite coherent in time to spatially homogeneous oscillations that on the other hand appear very irregular in time.

III. TIME-DELAYED FEEDBACK CONTROL

In order to control the noise-induced patterns considered in the previous section, we will use the method of time-delayed feedback which was previously applied successfully in deterministic chaos control of this particular system [23] as well as for control of noise-induced oscillations in simple models [20,21,25] without spatial degrees of freedom.

The voltage u is easily accessible in a real experiment. Therefore, as a simple and adaptive method of control, we add the time-delayed feedback only to the voltage variable u in Eq. (1),

$$\frac{\partial a(x,t)}{\partial t} = f(a,u) + \frac{\partial}{\partial x}\left(D(a)\frac{\partial a}{\partial x}\right) + D_a\xi(x,t),$$

$$\frac{\partial u(t)}{\partial t} = \frac{1}{\varepsilon}(U_0 - u - rJ) + D_u\eta(t) - K[u(t)-u(t-\tau)]. \tag{4}$$

By varying the control amplitude K, we can adjust the strength of the control force; τ is the time delay of the feedback loop.

A. Numerical simulations

To get a first impression of whether this control force is able to change the temporal regularity of the noise-induced oscillations, we fix $D_u=0.1$, $D_a=10^{-4}$, as in the middle panel of Fig. 2, and calculate the correlation time in dependence of the feedback strength K for two different delay times τ. From Fig. 4, one can see that the qualitative result depends strongly upon the choice of the delay time. While for $\tau=7$ the control loop strongly increases the correlation time with increasing K, it is on the other hand able to decrease it significantly for $\tau=5$. The same can be seen from Fig. 3. Here the control with $K=0.1$ and $\tau=7$ enhances the correlation time, compared with the uncontrolled case, over a relatively wide range of the noise intensity up to $D_u\approx 0.5$, whereas $\tau=5$ decreases it within the same range. The difference in regularity for different values of τ and K also shows up in the corresponding spatiotemporal patterns and voltage time series (Fig. 5), where (b) is clearly more regular than (a).

The role of the appropriate choice of the control delay τ becomes even clearer if we keep K fixed and calculate the correlation time in dependence of τ. The result is plotted in Fig. 6(a), where one can clearly see the oscillatory character of the correlation time under variation of τ, which is charac-

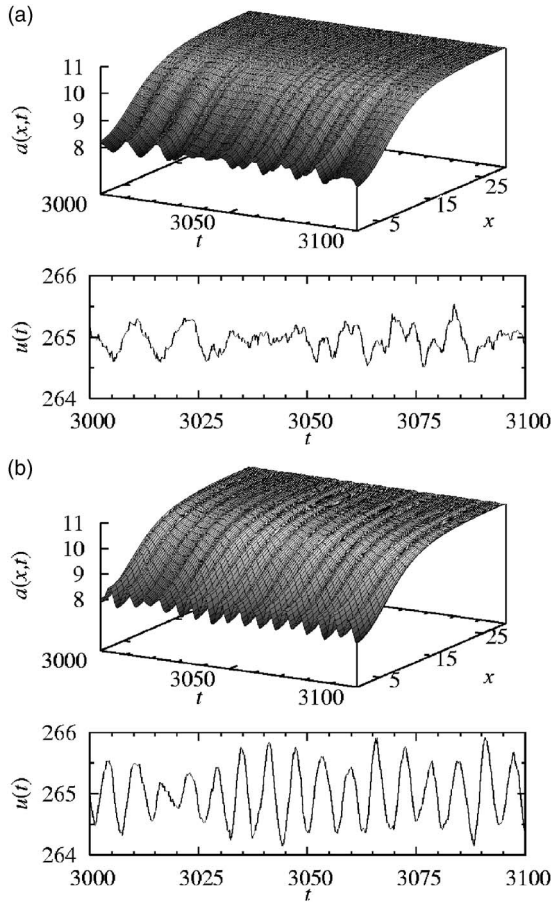

FIG. 5. Spatiotemporal patterns $a(x,t)$ and voltage time series $u(t)$ for different values of the control strength K and delay time τ. (a) $\tau=4.0$, $K=0.4$; (b) $\tau=13.4$, $K=0.1$. $D_u=0.1$, $D_a=10^{-4}$, and other parameters as in Fig. 2.

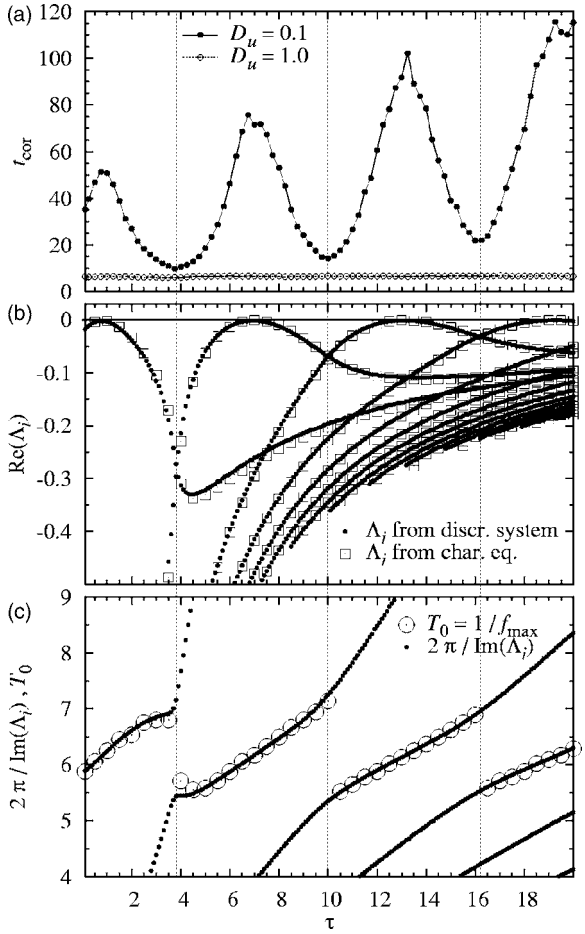

FIG. 6. (a) Correlation time [Eq. (3)] for two different noise intensities in dependence of the feedback delay τ. (b) Real parts of the eigenvalues Λ_i of the linearized deterministic system ($D_a=D_u=0$) calculated at the spatially inhomogeneous fixed point for $K=0.1$. The black dots are calculated from the spatially discretized system (set of ODEs) whereas the squares are calculated from Eq. (17) (see text). The vertical dotted lines mark values of τ at which the *leading* eigenvalue (i.e., the one with the largest real part) changes. (c) Eigenperiods $2\pi/\mathrm{Im}(\Lambda_i)$ of the deterministic system and basic periods $T_0 := 1/f_{\max}$ of the noise-induced oscillations, where $f_{\max}$ denotes the frequency of the highest peak in the Fourier power spectral density of the noisy system with $D_u=0.1$, $K=0.1$.

terized by the presence of "optimal" values of τ, corresponding to maximum regularity, and "worst" values of τ, which are related to minimum regularity of the noise-induced dynamics. At the same time it is shown that the control with $K=0.1$ produces no effect at all upon the correlation time if the noise is too large (lower curve for $D_u=1.0$).

The fact that noise-induced oscillations take place in the vicinity of the spatially inhomogeneous fixed point gives us a hint that some properties of these oscillations could relate to the stability of the above-mentioned fixed point. To gain some insight into how the control actually affects the systems dynamics around the spatially inhomogeneous fixed point, we linearize the system equations (4) for $D_u=D_a=0$ and calculate the eigenvalues Λ_i at the fixed point. First of all, we calculate these eigenvalues from the spatially discretized system which we use for the numerical simulation. This discretized version is just a set of ordinary differential equations (ODEs) and the linearization and the eigenvalues can be computed easily.

In Fig. 6(b), one can see that the control with $K=0.1$ does not change the stability of the inhomogeneous fixed point since the real parts of all eigenvalues do not become positive within the given range of τ. Nevertheless with increasing τ the real parts of the eigenvalue intersect at particular values of τ (vertical dotted lines) and therefore the *leading* eigenvalue, i.e., the "least stable" one or the one with the largest real part, changes at these values of τ. As one can see, these crossover points correspond to the minima of the correlation time in Fig. 6(a), whereas the local maxima of the real parts correspond to the maxima of the correlation time. This gives rise to a rather intuitive explanation for the behavior of the correlation time: The closer to zero the real part of an eigenvalues is, the weaker is the attracting stability of the fixed point and the easier it is for the noise to excite exactly the oscillating mode corresponding to this particular eigenvalue. On the other hand, at the intersection points of the real parts of the leading eigenvalue, these values have the largest distance from zero, meaning that the attracting stability of the fixed point is stronger and in addition there are two different corresponding oscillating modes that are excited by the

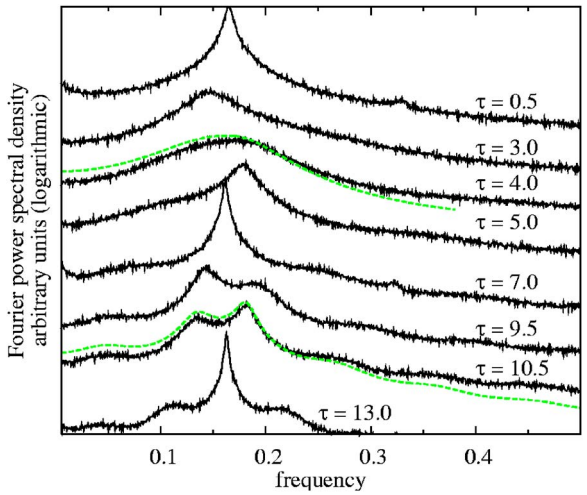

FIG. 7. (Color online) Fourier power spectral density of the dynamical variable $u(t)$. The different curves are shifted vertically for clarity. Averages from 100 time series of length $T=10\,000$ with $K=0.1$, $D_u=0.1$, $D_a=10^{-4}$, other parameters as in Fig. 2. Dashed (green) curves correspond to analytical approximation from Eq. (33).

noise. Thus the control cannot reach its optimal effect.

As a direct consequence, the main frequency that is activated by the noise switches exactly at these values of τ to the eigenfrequency of the corresponding leading eigenvalue. In Fig. 6(c), the eigenperiods are plotted as black dots in dependence of τ. The circles mark the positions of the highest peak in the Fourier power spectrum for the corresponding noisy system with $D_u=0.1$ (cf. Fig. 7). One can see clearly that these main periods switch from one branch to another exactly at the positions where the real parts of two different eigenvalues cross over; see, e.g., the curves for $\tau=9.5$ and 10.5 in Fig. 7.

In Fig. 6(a), we have seen that for larger noise intensity ($D_u=1.0$), the control seems to have no effect upon the temporal correlation of the oscillations. Furthermore, we know from the uncontrolled system that for increasing noise intensity the dynamics of the system without control tends to become more and more spatially homogeneous. In Fig. 8, we show the main periods of the oscillations in the controlled system with noise intensity $D_u=1.0$ (circles). One can see that they do not follow the eigenperiods of the linearized system at the inhomogeneous fixed point (black dots) as for small noise intensity in Fig. 6(c). Instead they turn out to be shifted toward the branches of the eigenperiods (triangles) of the spatially homogeneous, *reduced* system linearized at the homogeneous fixed point "H" from Fig. 1. This reduced system is just a system of two ODEs.

B. Analysis of the general form of the characteristic equation

As we have already noted in the previous section, the eigenvalues for the linearized deterministic system at the inhomogeneous fixed point, plotted as black dots in Figs. 6(b), 6(c), and 8, are computed numerically for the system (4) in the deterministic case by using the spatially discretized set of ordinary differential equations.

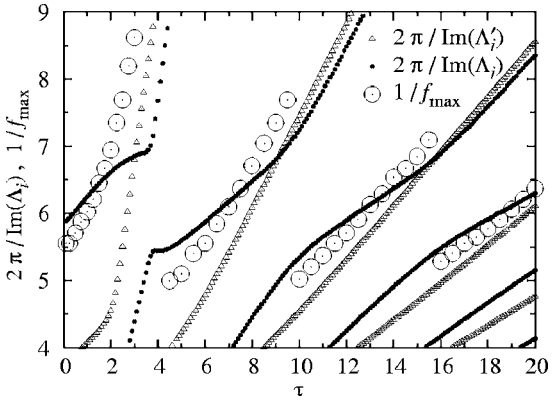

FIG. 8. Eigenperiods of the deterministic full system at the inhomogeneous fixed point $[2\pi/\mathrm{Im}(\Lambda_i)$, same as in Fig. 6(c)], eigenperiods of the reduced homogeneous system at the homogeneous fixed point $[2\pi/\mathrm{Im}(\Lambda_i')]$, and basic periods $T_0:=1/f_{\max}$ of the noise-induced oscillations, where $f_{\max}$ denotes the frequency of the highest peak in the Fourier power spectral density of the noisy system with $D_u=1.0$, $K=0.1$.

To achieve a deeper understanding of the stability properties of the inhomogeneous fixed point under the influence of the control force and to obtain the general form of the characteristic equation that determines the eigenvalues of this linearized system, we perform the linearization of the original continuous system (4) at the spatially inhomogeneous fixed point $(a_0(x),u_0)$. Introducing

$$a_x \equiv \frac{\partial a}{\partial x}, \quad a_{xx} \equiv \frac{\partial^2 a}{\partial x^2}, \tag{5}$$

$$b(a,a_x,a_{xx}) \equiv \frac{\partial}{\partial x}[D(a)a_x], \tag{6}$$

and a linear operator

$$\mathcal{L} \equiv \left.\frac{\partial f}{\partial a}\right|_{a_0,u_0} + \left.\frac{\partial b}{\partial a}\right|_{a_0} + \left.\frac{\partial b}{\partial a_x}\right|_{a_0}\frac{\partial}{\partial x} + \left.\frac{\partial b}{\partial a_{xx}}\right|_{a_0}\frac{\partial^2}{\partial x^2}, \tag{7}$$

and using the ansatz $\delta a(x,t)=e^{\Lambda t}\tilde{a}(x)$, $\delta u(t)=e^{\Lambda t}\tilde{u}$ for the deviations from the fixed point, we can write down the coupled eigenvalue problem,

$$\Lambda\tilde{a}(x) = \mathcal{L}\tilde{a}(x) + f_u(x)\tilde{u}, \tag{8}$$

$$\Lambda\tilde{u} = -\frac{r}{\varepsilon L}\int_0^L j_a(x)\tilde{a}(x)dx + \left[-\frac{1+rJ_u}{\varepsilon} + K(e^{-\Lambda\tau}-1)\right]\tilde{u},$$

$$\text{with } f_u \equiv \left.\frac{\partial f}{\partial u}\right|_{a_0,u_0}, \quad j_a \equiv \left.\frac{\partial j}{\partial a}\right|_{a_0,u_0},$$

$$J_u = \frac{1}{L}\int_0^L \left.\frac{\partial j}{\partial u}\right|_{a_0,u_0} dx. \tag{9}$$

For the case $K=0$, this eigenvalue problem of the inhomogeneous filamentary fixed point has been analyzed gener-

ally [26]. In the voltage-clamped case ($\delta u=0$), the Sturmian eigenvalue equation $\lambda\tilde{a}=\mathcal{L}\tilde{a}$ with Neumann boundary conditions (which can be shown to be self-adjoint) has solutions $\lambda_0>\lambda_1>\lambda_2>\cdots$, where the corresponding eigenmode $\psi_n(x)$ has n nodes, and $\lambda_0>0$, while all other eigenvalues $\lambda_n<0$ for $n\geqslant 1$ are stable. The eigenmodes of the full Eqs. (8) and (9) can be expanded in terms of the voltage-clamped eigenmodes,

$$\tilde{a}(x)=\sum_n (\tilde{a},\psi_n)\psi_n(x), \tag{10}$$

where $(\tilde{a},\psi_n)\equiv(1/L)\int_0^L\tilde{a}(x)\psi_n(x)dx$ denotes the usual scalar product in Hilbert space. Inserting this into Eq. (8) yields

$$\Lambda\sum_n (\tilde{a},\psi_n)\psi_n(x)=\sum_n \lambda_n(\tilde{a},\psi_n)\psi_n(x)+f_u(x)\tilde{u}. \tag{11}$$

Forming the scalar product with ψ_m and using orthonormality gives the expansion coefficients

$$(\tilde{a},\psi_m)=\frac{(f_u,\psi_m)}{\Lambda-\lambda_m}\tilde{u}. \tag{12}$$

The expansion (10) can be inserted into Eq. (9),

$$\Lambda\tilde{u}=\left[-\frac{r}{\varepsilon}\sum_n\frac{(f_u,\psi_n)(j_a,\psi_n)}{\Lambda-\lambda_m}-\frac{1+rJ_u}{\varepsilon}+K(e^{-\Lambda\tau}-1)\right]\tilde{u}. \tag{13}$$

We will now neglect the higher modes ψ_n because they oscillate fast whereas $a_0(x)$ varies slowly in space, and we approximate the sum in Eq. (10) by the dominant first term ψ_0 with $\lambda_0>0$. We obtain the characteristic equation for the eigenvalue Λ,

$$\Lambda^2+\left(\frac{1+rJ_u}{\varepsilon}-\lambda_0\right)\Lambda+(\lambda_0-\Lambda)K(e^{-\Lambda\tau}-1)-\frac{\lambda_0}{\varepsilon}(1+r\sigma_d)=0, \tag{14}$$

where the static differential conductance at the inhomogeneous fixed point

$$\sigma_d\equiv\left.\frac{dJ}{du}\right|_{a_0,u_0}=J_u+\left(j_a,\frac{da}{du}\right)=J_u-(j_a,\psi_0)\frac{(f_u,\psi_0)}{\lambda_0} \tag{15}$$

has been introduced using Eqs. (10) and (12) in the static case $\Lambda=0$ [1]. Without control, $K=0$, Eq. (14) reduces to a characteristic polynomial of second order, which gives the well-known conditions for stability of a filament [26],

$$A\equiv\frac{1+rJ_u}{\varepsilon}-\lambda_0>0,$$

$$C\equiv-\frac{\lambda_0}{\varepsilon}(1+r\sigma_d)>0. \tag{16}$$

Without control, a Hopf bifurcation on the two-dimensional center manifold occurs if $A=0$. With control, Eq. (14) can be expressed as

$$\Lambda^2+A\Lambda+(B-\Lambda)K(e^{-\Lambda\tau}-1)+C=0 \tag{17}$$

with $B\equiv\lambda_0>0$. The parameters A, B, C can be calculated directly from Eq. (16). For the inhomogeneous fixed point, $\lambda_0=1.0281$ has been calculated in [27]; $J_u=-0.1615$ can be obtained by using the condition for a Hopf bifurcation ($A=0$) in Eq. (16); $\sigma_d=0.226$ can be estimated from the current-voltage characteristic shown in Fig. 1.

This yields $A=0.0447$, $B=1.0281$, and $C=1.1458$. Note that in dimensional units, the unstable eigenvalue of the voltage-clamped system $\lambda_0=B$ is approximately equal to the inverse tunneling time $1/\tau_a$. With these values we can solve Eq. (17). For $K=0.1$, the real parts of this solution in dependence of τ are also shown in Fig. 6(b) as squares. They coincide with very good accuracy.

Let us now write $\Lambda=p+iq$ with $p,q\in\mathbb{R}$ and separate Eq. (17) into real and imaginary parts,

$$\text{Re: } p^2-q^2+Ap+K[p-B+(B-p)e^{-p\tau}\cos(q\tau)-qe^{-p\tau}\sin(q\tau)]=0, \tag{18}$$

$$\text{Im: } 2pq+Aq+K[q-(B-p)e^{-p\tau}\sin(q\tau)-qe^{-p\tau}\cos(q\tau)]=0. \tag{19}$$

To estimate the maxima of $p=\mathrm{Re}(\Lambda)$ in dependence of the control delay τ (to find the "optimal" delay), we assume $p\approx 0$ (but $p\neq 0$!), $K\ll 1$, and use Eq. (19),

$$2pq+Aq+Kq-KB\sin(q\tau)-Kq\cos(q\tau)=0, \tag{20}$$

$$\Leftrightarrow 2p=K\left(\frac{B}{q}\sin(q\tau)+\cos(q\tau)\right)-A-K, \tag{21}$$

$$\Leftrightarrow 2p=K\sqrt{\left(\frac{B}{q}\right)^2+1}\cos\left[q\tau-\arctan\left(\frac{B}{q}\right)\right]-A-K. \tag{22}$$

Hence, p has a maximum if

$$q\tau-\arctan\left(\frac{B}{q}\right)=2\pi n,\quad n\in\mathbb{Z}. \tag{23}$$

Since $q=\mathrm{Im}(\Lambda)\approx 1$ in the vicinity of the maxima of p [cf. Fig. 6(c)] and also $B\approx 1$, we get

$$\tau=2\pi n+\frac{\pi}{4}. \tag{24}$$

According to this simple formula, the first four maxima of $p=\mathrm{Re}(\Lambda)$ appear at $\tau\approx 0.8$, 7.1, 13.4, and 19.6, which is in very good agreement with Fig. 6(b).

Next, we consider the eigenvalues at larger values of τ, i.e., $\tau\gg 1$, $p\approx 0$, $q\neq 0$, in Eq. (19),

$$\cos\left[q\tau-\arctan\left(\frac{B}{q}\right)\right]\sqrt{\left(\frac{B}{q}\right)^2+1}=\frac{A+K}{K}. \tag{25}$$

This, with $A\approx 0$ and again $B/q\approx 1$, yields

$$\cos\left(q\tau-\frac{\pi}{4}\right)=\frac{1}{\sqrt{2}}, \tag{26}$$

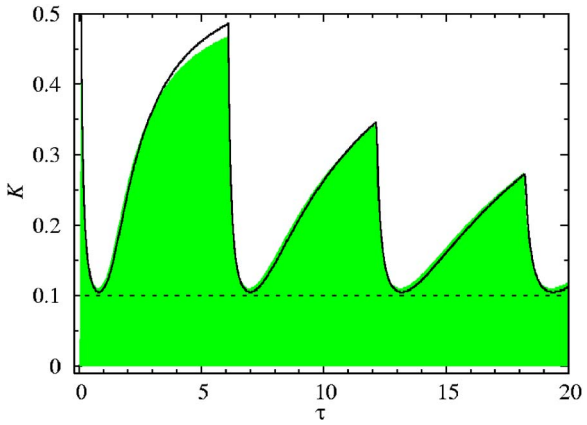

FIG. 9. (Color online) Stability regime in the τ-K plane of the deterministic system (4), $D_u=D_a=0$. The area below the curve marks the regime within which the inhomogeneous fixed point is still stable under the influence of the control loop. Within the upper regime, the fixed point is unstable. The shaded (green) area is calculated from the space-discretized system of ODEs, whereas the black curve is calculated from Eq. (17). The dotted line corresponds to the upper bound of K given in Eq. (30).

$$\Leftrightarrow q\tau - \frac{\pi}{4} = \frac{\pi}{4} + 2\pi n, \quad n \in \mathbb{Z}. \tag{27}$$

Hence we arrive at an estimate for the period $T=2\pi/q$,

$$T = \frac{4\tau}{1+4n}, \tag{28}$$

which describes the piecewise linear behavior of the eigenperiods for larger τ with again very good agreement.

Finally, we investigate the condition for a Hopf bifurcation (i.e., $p=0$, $q\neq 0$) in dependence of K. Equation (25) together with $B/q \approx 1$ yields

$$\cos\left(q\tau - \frac{\pi}{4}\right) = \frac{A+K}{K\sqrt{2}}. \tag{29}$$

If the right-hand side is larger than unity, no solution exists and thus no Hopf bifurcation and no instability of the fixed point can occur,

$$\frac{A+K}{K\sqrt{2}} > 1 \Leftrightarrow K < \frac{A}{\sqrt{2}-1} \approx 0.1. \tag{30}$$

This determines a lower bound for the maximum control strength which we are not allowed to exceed as long as we do not want to lose the original stability of the fixed point. This maximum is perfectly confirmed in Fig. 9 where the regime is plotted, in which the inhomogeneous fixed point remains stable under the influence of the control term. Here one can see the very good match between the stability regime calculated on the one hand from the space discretized system of ODEs (shaded area) and on the other hand from our general characteristic equation (17) (black curve).

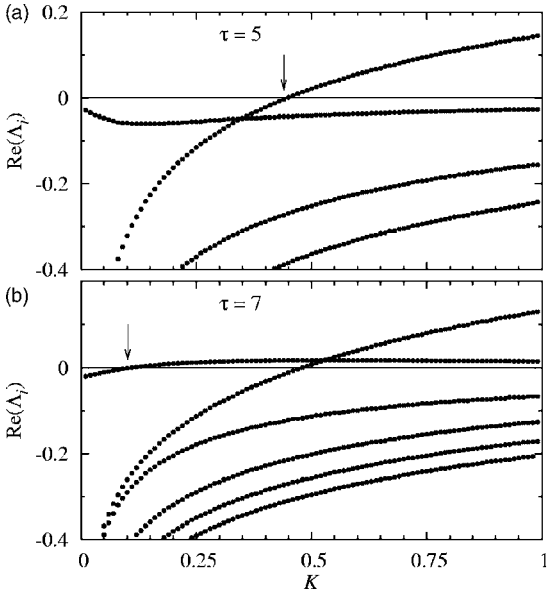

FIG. 10. Real parts of the eigenvalues Λ_i of the linearized deterministic system with (a) $\tau=5$ and (b) $\tau=7$. The arrows mark Hopf bifurcations.

An analytical estimation of the power spectral density is available along the same lines as in [28]. Namely, we can approximate the noise-induced oscillations of u using the linearized dynamical equation (with effective noise intensity $D' \ll 1$), which corresponds to the characteristic Eq. (17),

$$\frac{\partial^2 u(t)}{\partial t^2} + A\frac{\partial u(t)}{\partial t} + BK[u(t-\tau)-u(t)] - K\left(\frac{\partial u(t-\tau)}{\partial t} - \frac{\partial u(t)}{\partial t}\right) + Cu(t) = D'\xi(t). \tag{31}$$

Applying a Fourier transform to Eq. (31) yields

$$-\omega^2\hat{u} - iA\omega\hat{u} + (B+i\omega)K\hat{u}(e^{i\omega\tau}-1) + C\hat{u} = D'\hat{\xi}(\omega), \tag{32}$$

where $\hat{u}(\omega)$ is the Fourier image of $u(t)$. Then we obtain the power spectral density

$$S_{uu}(\omega) = \frac{D'^2}{2\pi}(\{-\omega^2 + C + KB[\cos(\omega\tau)-1] - \omega K\sin(\omega\tau)\}^2 + \{KB\sin(\omega\tau) + \omega K[\cos(\omega\tau)-1] - \omega A\}^2)^{-1}. \tag{33}$$

In Fig. 7, two curves of $S_{uu}(2\pi f)$ for $\tau=4$ and 10.5 are plotted. As one can see, they agree very well with the numerically estimated power spectra.

C. Delay-induced oscillatory patterns

So far we have kept the control amplitude fixed and varied the control delay τ. But as we have already seen in Fig. 9, the control force can in principle change the deterministic behavior of the system. This is shown in Fig. 10. One can see that the spatially inhomogeneous fixed point undergoes a Hopf bifurcation around $K=0.5$ for $\tau=5$. For $\tau=7$, another eigenvalue becomes positive already at $K\approx 0.1$. Thus for a

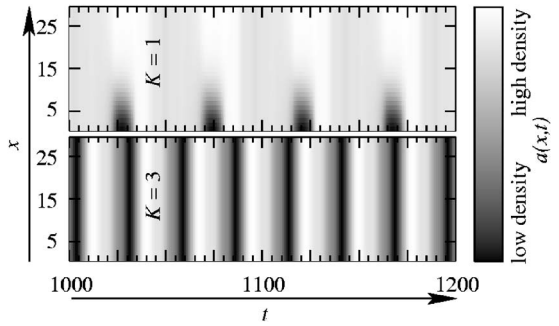

FIG. 11. Delay-induced periodic patterns: Spatiotemporal patterns $a(x,t)$ of the controlled deterministic system (4) with $\tau=7$ for $K=1$ and $K=3$. $D_u=D_a=0$, other parameters as in Fig. 2.

given τ and sufficiently high K, the control loop changes the deterministic dynamics of our system: The previously stable fixed point exhibits a Hopf bifurcation, becomes unstable, and a stable periodic spatiotemporal pattern is induced in the system by the control loop. With increasing K, the shape of this induced periodic breathing pattern changes from small spatially inhomogeneous oscillations around the previously stable fixed point into a spatiotemporal spiking pattern (Fig. 11, upper panel) and further into a completely spatially homogeneous oscillation (Fig. 11, lower panel). To see whether or not the deterministic spiking behavior still persists under the influence of noise, we have added different noise intensities to the system at $K=1$. The result is shown in Fig. 12 and one can see that again increasing noise renders the dynamics more and more spatially homogeneous even though there exists a deterministic stable limit cycle corresponding to a spiking pattern.

IV. CONCLUSION

We have investigated the effect of a time-delayed feedback control loop upon the complex spatiotemporal behavior of the double-barrier resonant tunneling diode just below the Hopf bifurcation point under the influence of Gaussian white noise.

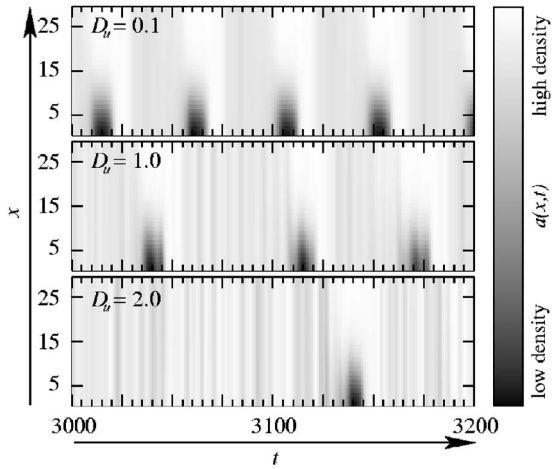

FIG. 12. Spatiotemporal patterns $a(x,t)$ of the controlled system (4) with noise, $K=1.0$, $\tau=7.0$, $D_a=10^{-4}$, D_u as indicated, other parameters as in Fig. 2.

It was shown that delayed feedback can be an efficient method for manipulation of essential characteristics of noise-induced spatiotemporal dynamics in a semiconductor nanostructure. By variation of the time delay, one can deliberately adjust the time scale of oscillatory patterns of the lateral current density distribution, and thus adjust the frequency of the device. Moreover, with a proper choice of feedback parameters, one can also effectively control the coherence of spatiotemporal dynamics, e.g., enhance or destroy it. Increase of coherence is possible up to a reasonably large intensity of noise. However, as the level of noise grows, the efficiency of the control upon the temporal coherence decreases.

The effects of the delayed feedback can be explained in terms of a linear stability analysis. For this purpose, we have derived the general form of the characteristic equation for the deterministic system (4) close to but below a Hopf bifurcation. Both dependencies, coherence and time scale versus τ, demonstrate an oscillatory character, which can be explained by oscillations of the real and imaginary parts of the eigenvalues of the linearized system at the fixed point, in the vicinity of which the noise-induced oscillations occur. The most coherent time scale corresponds to values of τ, for which the real parts of the eigenvalues attain a maximum. In some sense, the noise excites the least stable eigenmode: the less stable an eigenmode is, the greater is the coherence of the corresponding oscillations. Analogously, the dependence of the time scale versus τ just reproduces the piecewise linear character of the inverse imaginary part of the eigenvalues as τ changes. If the noise intensity increases, the phase trajectory spends more time in the vicinity of the second (homogeneous but unstable) fixed point. The time scales of the noise-induced motion then become influenced by the local stability properties of this fixed point (cf. Fig. 8).

For larger K, the time-delayed feedback is able to induce a Hopf bifurcation that gives rise to deterministic periodic oscillations, whose spatial properties are determined by the values of K: the larger K, the more homogeneous the oscillations appear. If these delay-induced deterministic oscillations are spatially inhomogeneous, the increase of the noise amplitude in the system again renders them more and more homogeneous.

ACKNOWLEDGMENTS

This work was supported by DFG in the framework of Sfb 555. The authors are grateful to G. Bordiougov and N. Janson for fruitful discussions.

APPENDIX

The effective diffusion coefficient $D(a)$ results from the inhomogeneous lateral redistribution of carriers and from the change in the local potential due to the charge accumulated in the quantum well by Poisson's equation [12],

$$D(a) = a\left(\frac{d}{r_B} + \frac{1}{1-\exp(-a)}\right), \tag{A1}$$

where d is the effective thickness of the double-barrier structure, $r_B=(4\pi\epsilon\epsilon_0\hbar^2)/(e^2m)$ is the effective Bohr radius in the semiconductor material, and ϵ and ϵ_0 are the relative and absolute permittivity of the material.

From microscopic consideration of the tunneling currents from the emitter into the quantum well and from there to the emitter, one obtains the function f [14],

$$f(a,u) = \left\{\frac{1}{2} + \frac{1}{\pi}\arctan\left[\frac{2}{\gamma}\left(x_0 - \frac{u}{2} + \frac{d}{r_B}a\right)\right]\right\} \times\left\{\ln\left[1+\exp\left(\eta_e - x_0 + \frac{u}{2} - \frac{d}{r_B}a\right)\right] - a\right\} - a. \tag{A2}$$

x_0 and γ describe the energy level and the broadening of the electron states in the quantum well and η_e is the dimensionless Fermi level in the emitter, all in units of k_BT. Throughout the paper, we use values of $\gamma=6$, $d/r_B=2$, $\eta_e=28$, and $x_0=114$.

[1] E. Schöll, *Nonlinear Spatio-temporal Dynamics and Chaos in Semiconductors* (Cambridge University Press, Cambridge, 2001).
[2] L. L. Chang, L. Esaki, and R. Tsu, Appl. Phys. Lett. **24**, 593 (1974).
[3] V. J. Goldman, D. C. Tsui, and J. E. Cunningham, Phys. Rev. Lett. **58**, 1256 (1987).
[4] A. D. Martin, M. L. F. Lerch, P. E. Simmonds, and L. Eaves, Appl. Phys. Lett. **64**, 1248 (1994).
[5] A. Wacker and E. Schöll, J. Appl. Phys. **78**, 7352 (1995).
[6] E. Özbay, D. M. Bloom, and S. K. Diamond, Electron. Lett. **26**, 1046 (1990).
[7] K. L. Jensen and F. A. Buot, Phys. Rev. Lett. **66**, 1078 (1991).
[8] B. A. Glavin, V. A. Kochelap, and V. V. Mitin, Phys. Rev. B **56**, 13346 (1997).
[9] D. Mel'nikov and A. Podlivaev, Semiconductors **32**, 206 (1998).
[10] M. N. Feiginov and V. A. Volkov, JETP Lett. **68**, 662 (1998).
[11] M. Meixner, P. Rodin, E. Schöll, and A. Wacker, Eur. Phys. J. B **13**, 157 (2000).
[12] V. Cheianov, P. Rodin, and E. Schöll, Phys. Rev. B **62**, 9966 (2000).
[13] P. Rodin and E. Schöll, J. Appl. Phys. **93**, 6347 (2003).
[14] E. Schöll, A. Amann, M. Rudolf, and J. Unkelbach, Physica B **314**, 113 (2002).
[15] Y. M. Blanter and M. Büttiker, Phys. Rep. **336**, 1 (2000).
[16] G. Giacomelli, M. Giudici, S. Balle, and J. R. Tredicce, Phys. Rev. Lett. **84**, 3298 (2000).
[17] V. V. Sherstnev, A. Krier, A. G. Balanov, N. B. Janson, A. N. Silchenko, and P. V. E. McClintock, Fluct. Noise Lett. **1**, 91 (2003).
[18] O. Ushakov, H. J. Wünsche, F. Henneberger, I. A. Khovanov, L. Schimansky-Geier, and M. Zaks, Phys. Rev. Lett. **95**, 123903 (2005).
[19] G. Stegemann, A. G. Balanov, and E. Schöll, Phys. Rev. E **71**, 016221 (2005).
[20] N. B. Janson, A. G. Balanov, and E. Schöll, Phys. Rev. Lett. **93**, 010601 (2004).
[21] A. G. Balanov, N. B. Janson, and E. Schöll, Physica D **199**, 1 (2004).
[22] K. Pyragas, Phys. Lett. A **170**, 421 (1992).
[23] J. Unkelbach, A. Amann, W. Just, and E. Schöll, Phys. Rev. E **68**, 026204 (2003).
[24] R. L. Stratonovich, *Topics in the Theory of Random Noise* (Gordon and Breach, New York, 1963), Vol. 1.
[25] J. Pomplun, A. Amann, and E. Schöll, Europhys. Lett. **71**, 366 (2005).
[26] A. Alekseev, S. Bose, P. Rodin, and E. Schöll, Phys. Rev. E **57**, 2640 (1998).
[27] J. Unkelbach, Master's thesis, TU Berlin, 2002.
[28] E. Schöll, A. Balanov, N. B. Janson, and A. Neiman, Stochastics Dyn. **5**, 281 (2005).